The thermal decomposition of hydronium jarosite and ammoniojarosite

Henry Spratt,[1] Llew Rintoul,[1] Maxim Avdeev[2] and Wayde Martens[1]*

[1]*Chemistry, Physics and Mechanical Engineering, Science and Engineering Faculty, Queensland University of Technology, Brisbane, Queensland 4001, Australia*

[2]*Bragg Institute, Australian Nuclear Science and Technology Organisation, Lucas Heights, NSW 2234, Australia*

*Corresponding author (ph: +61 7 3138 2472, email: w.martens@qut.edu.au

Abstract The thermal decomposition of hydronium jarosite and ammoniojarosite was studied using thermogravimetric analysis and mass spectrometry, *in situ* synchrotron X-ray diffraction and infrared emission spectroscopy. There was no evidence for the simultaneous loss of water and sulfur dioxide during the desulfonation stage as has previously been reported for hydronium jarosite. Conversely, all hydrogen atoms are lost during the dehydration and dehydroxylation stage from 270 to 400 °C and no water, hydroxyl groups or hydronium ions persist after 400 °C. The same can be said for ammoniojarosite. The first mass loss step during the decomposition of hydronium jarosite has been assigned to the loss of the hydronium ion via protonation of the surrounding hydroxyl groups to evolve two water molecules. For ammoniojarosite, this step corresponds to the protonation of a hydroxyl group by ammonium, so that ammonia and water are liberated simultaneously. Iron(II) sulfate was identified as a possible intermediate during the decomposition of ammoniojarosite (421–521 °C) due to a redox reaction between iron(III) and the liberated ammonia during decomposition. Iron(II) ions were also confirmed with the 1,10-phenanthroline test. Iron(III) sulfate and other commonly suggested intermediates for hydronium and ammoniojarosite decomposition are not major crystalline phases; if they are formed, then they most likely exist as an amorphous phase or a different low temperature phases than usual.

Keywords: hydronium jarosite, ammoniojarosite, thermal decomposition, iron(III) reduction

Introduction

The alunite supergroup of minerals has the general formula $AB_3(SO_4)_2(OH)_6$ and is a large group of minerals. The A site is typically occupied by a monovalent cation, while a trivalent cation is commonly at the B site. Jarosites (Fe^{3+} at the B site) are used to precipitate iron (Fe) and alkali metals from metallurgical solutions in the zinc, copper, and lead industries [1]. Jarosite minerals are also by-products of some metal processing industries and the mining industry [2]. As hydronium jarosite (H_3O^+ at the A site) and ammoniojarosite (NH_4^+ at the A site) contain no alkali metals, they could be used to produce pure hematite (Fe_2O_3) via calcination for applications such as pigments, catalysts, magnetic materials, and clinker production [3-5].

The thermal decomposition of sulfate minerals, including jarosites, has been studied for some time using thermogravimetric analysis (TG) [6-9]. In many cases, X-ray diffraction (XRD) patterns are also collected [10-13], but these patterns are frequently complex, and phase identification is not always possible [8]. The intermediate products formed during the decomposition of other jarosite minerals are well characterized [12-14]. Infrared emission spectroscopy (IES), though infrequently used, has been shown to be useful for the study of sulfate minerals at high temperature and offers additional information to TG and XRD [15].

The decomposition of jarosite minerals proceeds in two distinct steps: dehydration and dehydroxylation at temperatures between 250 and 450 °C via the loss of H_2O; and desulfonation at temperatures between 600 and 800 °C via the loss of SO_3 which then decomposes to SO_2 and SO. The onset temperature of dehydroxylation and dehydration is dependent on the A site cation [3]. The final decomposition product depends on the A site cation, but is usually hematite [5, 7], hematite and ASO_4 where A is the A site cation [7, 13, 16], or hematite and the A site metal as is the case with argentojarosite [$AgFe_3(SO_4)_2(OH)_6$] [8].

Different mechanisms for the thermal decomposition of hydronium jarosite have been proposed in the few studies, which focuses on this mineral [3, 17-19]. Frost et al. [17] and Šolc et al. [19] believe that the hydronium ion (H_3O^+) persists in the structure at high temperature and that one mol of both H_2O and SO_3 are lost simultaneously at ~557 °C. This is in contrast with other results from the literature, which suggest that the first decomposition step is the loss of H_3O^+ from the crystal structure and the dehydration and desulfonation occur in two distinct steps [3, 18]. The intermediate compounds after dehydroxylation and dehydration proposed by these two authors also differ.

Kubisz [3] argued that there are four types of dehydration and dehydroxylation reactions: deprotonation, dehydration, main dehydroxylation, and final dehydroxylation which form a variety of Fe oxy/hydroxy/hydrated sulfate complexes and/or hematite. Deprotonation i.e, $H_3O^+ \rightarrow H_2O + H^+$, occurs at about 320 °C and movement of the proton to hydroxyl oxygen atoms is more likely

than the protonation of sulfate oxygen atoms (assuming an analogy to $[H_3OGa_3(SO_4)_2(OH)_6]$) [3]. This mechanism differs to Frost et al. [17] who have this particular proton moving to sulfate groups to evolve H_2O and SO_2 at 557 °C. There is also another dehydration reaction that occurs between 520 and 550 °C [3]. This reaction is the dehydration of hydroxyl containing Fe sulfate compounds formed during the main dehydroxylation/dehydration stage and liberation of H_2O that is trapped in the jarosite structure. Following this, desulfonation occurs as usual with the eventual product being hematite.

The decomposition of ammoniojarosite has been studied [4, 5, 7, 11, 12, 20, 21], but more work is needed to identify intermediate products from its thermal decomposition. There is agreement in the literature [5, 7, 11] that the general scheme for the decomposition of ammoniojarosite is as follows: evolution of coordinated water; decomposition of ammoniojarosite to ferric sulfate and hematite via the loss of water and ammonia (NH_3); and lastly, formation of hematite as a result of the decomposition of Fe(III) sulfate.

This study examines the thermal analysis of ammoniojarosite and hydronium jarosite using IES, *in situ* synchrotron XRD and TG/MS. The dehydration and dehydroxylation stages as well as the loss of H_3O^+ from hydronium jarosite are of particular interest. This is due to the varying mechanisms presented during this stage of thermal decomposition. In addition it remains to be seen whether there is diffraction evidence for the intermediate compounds that have been previously proposed.

Experimental

Synthesis

Hydronium jarosite and ammoniojarosite were synthesized hydrothermally in Teflon-lined pressure vessels and heated in a microwave reactor for 3 h at 150 °C under autogenous water vapor pressure (4 bar). The synthesis of hydronium jarosite employed hydrous ferric sulfate ($Fe_2(SO_4)_3{\cdot}7H_2O$, 9 g) which was dissolved in H_2O (18.2 MΩ, 65 mL). The synthesis of ammoniojarosite used a high chloride concentration which has been shown to inhibit H_3O^+ substitution [22]. In this synthesis, ammonium chloride (NH_4Cl, 0.36 g) was added to a saturated lithium chloride (LiCl, 18 mL) and 1.23 M ferric chloride ($FeCl_3$, 7.5 mL) solution. Then, an excess of $Fe_2(SO_4)_3{\cdot}7H_2O$ (9 g) was dissolved in H_2O (18.2 MΩ, 38 mL) and added to the previous solution. After synthesis the products were thoroughly washed with water and dried in an oven overnight at 100 °C.

Chemical composition

Iron (Fe) and sulfur (S) contents were determined using a Varian inductively coupled plasma optical emission spectrometer (ICP-OES). Samples (c.a. 0.0072 g) were dissolved in concentrated nitric acid (HNO_3, 2.15 mL) at 120 °C followed by dilution to 50 mL with water (18.2 MΩ).

Various Fe (500 ppm) and S (1000 ppm) standards were prepared by serial dilution and made up in 3% HNO_3 for analysis. The S standard was spec pure sulfuric acid (H_2SO_4) and an ACR multi element standard was used as the Fe standard. The errors in the Fe and S contents are reported as the standard deviation from triplicate analyses. The S content was normalized to two in accordance with the literature for chemical formula calculations [23].

The nitrogen content of ammoniojarosite (c.a. 0.6 g) was determined using a Leco Trumac CN Analyzer operating at ~1,150 °C. Ceramic boats were used for the analysis with empty boats as a blank to check for drift. Ethylenediaminetetraacetic acid (EDTA, c.a. 0.2 g) was used as a standard. All measurements were run in triplicate and the error in nitrogen content reported as the standard deviation.

Thermogravimetric analysis

Thermogravimetric analysis was conducted on a TA instruments Q500 thermogravimetric analyzer under a nitrogen (N_2) atmosphere for hydronium jarosite and an argon (Ar) atmosphere for ammoniojarosite. An Ar atmosphere was used for ammoniojarosite analyses to enable detection of nitrogen had it been evolved. In both cases, the furnace was purged at 10 mL min^{-1}. Approximately 45 mg of hydronium jarosite and 36 mg of ammoniojarosite were heated in a platinum (Pt) crucible from ambient temperature (c.a. 25 °C) to 1,000 °C at a rate of 5 °C min^{-1}. Evolved gas analysis was performed with a Balzers (Pfeiffer) mass spectrometer (MS).

Infrared emission spectroscopy

Infrared emission spectroscopy was performed using a Nicolet Nexus FTIR spectrometer which was modified to include an emission cell. Heating was conducted *in situ* under a flowing N_2 atmosphere. Emission spectra were collected in the temperature range of 100–750 °C in 50 °C increments on a Pt stage. Details of the technique and the instrumentation employed in this study have been previously published [24, 17].

Synchrotron X-ray diffraction

Synchrotron XRD patterns were collected at the powder diffraction beam line of the Australian Synchrotron. Samples were loaded into quartz capillaries (0.5 mm) and patterns were collected in the temperature range of 25 °C–700 °C in 50 °C increments with heating provided by a hot air blower *in situ*. The detector was a Mythen microstrip detector. Unlike TGA and IES experiments, the atmosphere was not controlled and is best described as a closed air environment. The wavelength was determined to be 0.77308 Å via refinement of a LaB_6-660c/diamond standard. The data were then converted into intensity versus Cu Kα1 °2θ for phase analysis and identification purposes using the Bragg equation.

Results and discussion

Hydronium jarosite thermal decomposition

ICP-OES gave a Fe content of 3.13 ± 0.01 in the chemical formula after S normalization to two. The additional 0.13 (~4 %) Fe content is most likely due to another Fe containing phase in the sample. However, such a phase is below the level of detection of the diffractometer employed as no impurities are detected from room temperature to 218 °C, or the extra phase is amorphous. Thus, the authors consider that the hydronium jarosite phase in this sample has no Fe vacancies. Thermogravimetric (TG) and differential thermogravimetric (DTG) curves (Fig. 1) indicate that the decomposition of hydronium jarosite occurs in five main steps: 256, 339, 380, 560, and 603 °C. The mass losses associated with these temperatures are 8, 2, 5, 10 and 20 % respectively, resulting in a total mass loss of 45 %. The theoretical decomposition of hydronium jarosite to hematite results in a mass loss of 50 %, which is a difference of 5 % from the observed. Thus, the extra 5 % mass remaining from the observed TG results agrees with an amorphous Fe containing phase.

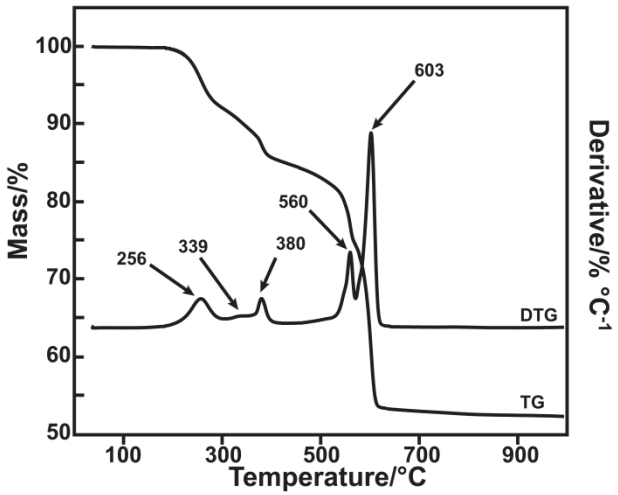

Fig. 1 TG/DTG curves for hydronium jarosite

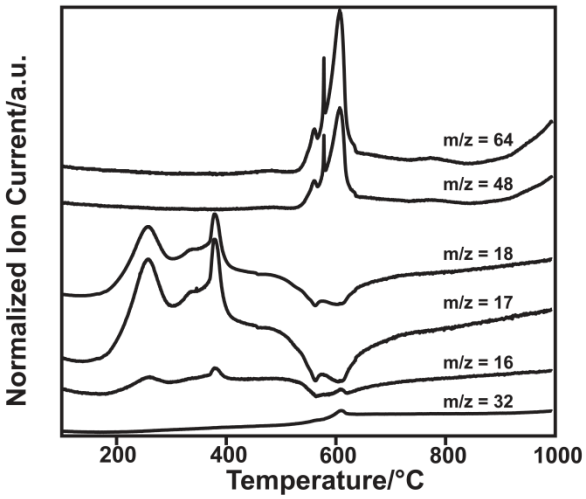

Fig. 2 MS of evolved gases for hydronium jarosite

From the mass spectra of evolved gases (Fig. 2), it is clear that the mass loss steps at 256, 339 and 380 °C are due to dehydroxylation and dehydration as H_2O (*m/z* = 18), OH (*m/z* = 17) and O (*m/z* = 16) are detected in this range by MS. From Fig. 2, it is also clear that desulfonation occurs at 560 and 603 °C due to the detection of SO_2 (*m/z* = 64), SO (*m/z* = 48), O and S (*m/z* = 32). Full decomposition is completed by 700 °C with dehydroxylation completed by 450 °C.

Figure 3 shows those XRD patterns where there is a change in the diffracting material for hydronium jarosite. At 720 °C, only hematite remains as the pattern is due solely to this phase. From the temperatures examined, hydronium jarosite is stable up to 218 °C before peaks due to another phase are seen at 270 °C, along with some unreacted hydronium jarosite. At 321 °C (after the first mass loss event, but before the second from TG), the pattern is solely due to this new phase.

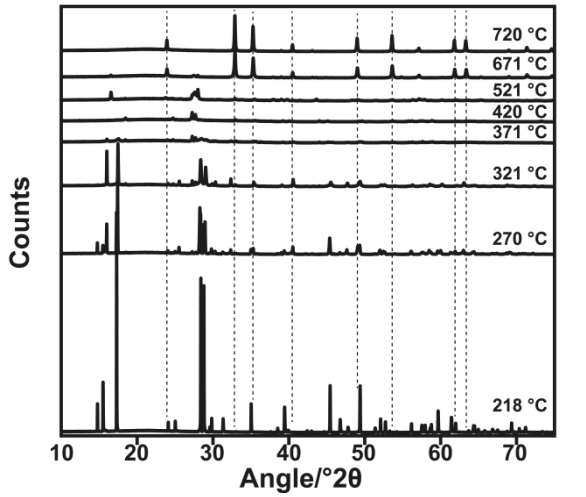

Fig. 3 Significant *in situ* synchrotron XRD patterns (converted to 1.54056 Å) of hydronium jarosite as a function of temperature. Most intense hematite peaks are marked by a dashed line

The mass loss of 8 % at 256 °C can be assigned to the loss of $2H_2O$ from hydronium jarosite (theoretical mass loss 7.5 %). This is most likely due to the protonation of a surrounding hydroxyl group by H_3O^+ which evolves $2H_2O$, in accordance with Kubisz [3]. The phase formed after the loss of $2H_2O$ was not positively identified using the PDF-4 database. However, this phase is most likely an Fe(III) hydroxy-sulfate of some description. Assuming the pattern at 321 °C is due to this phase alone, indexing of the first 24 significant peaks using the DICVOL 91 program within the Reflex module of Materials Studio (version 6) suggests that this phase is monoclinic with figures of merit (FOM) > 10. The first mass loss is tentatively assigned to the following reaction:

$$H_3OFe_3(SO_4)_2(OH)_6 \xrightarrow{256^{\circ}C} Fe_3(SO_4)_2(OH)_5 + 2H_2O$$

The theoretical loss of $1H_2O$ from hydronium jarosite is 3.75 %. The mass loss steps at 340 and 380 °C (2 and 5 % respectively) most likely represent the evolution of ~$0.5H_2O$ and $2H_2O$ as the total mass loss due to dehydroxylation and dehydration (15 %) agrees well with the theoretical loss of $4.5H_2O$ from hydronium jarosite (16.9 %). The five OH groups that remain after the first mass loss event would logically decompose and evolve $2.5H_2O$ to maintain charge balance. From Fig. 2 it is clear that no H_2O or OH is released after 450 °C. This suggests that dehydroxylation is separate to desulfonation.

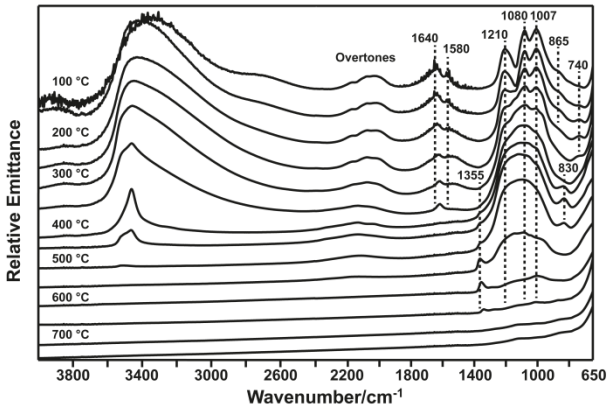

Fig. 4 IES spectra of hydronium jarosite (4,000 – 650 cm^{-1})

Figure 4 shows that there are no OH stretching bands present past 500 °C for OH bands. In addition, the bands at 1,640 and 1,580 cm^{-1} which have been attributed to O–H vibrations with the latter from H_3O^+ [25-27], have disappeared by 400 °C. As desulfonation begins at about 500 °C, there is little evidence for the persistence of hydronium ions and hydrogen atoms past dehydroxylation and dehydration as seen in some mechanisms [17, 19]. There is a gradual rise in the DTG curve from 400 to 500 °C and some weak OH IES bands in this temperature range. The extra step in hydronium jarosite decomposition proposed by Kubisz [3] most likely accounts for these two observations i.e., the gradual release of H_2O trapped in the jarosite structure and the full

dehydroxylation/dehydration of any unreacted intermediates due to temperature differences in the sample [3].

Previous studies indicate that what remains after dehydroxylation/dehydration (typically temperatures between 400 and 500 °C) is hematite, Fe(III) sulfate [$Fe_2(SO_4)_3$], Fe(II) sulfate ($FeSO_4$), $Fe_2O(SO_4)_2$ and/or various hydroxy-sulfate intermediates [3, 17-19]. Given the limited evidence for the presence of hydrogen atoms after dehydroxylation, hydroxy-sulfate compounds can be ruled out. Interestingly, the synchrotron XRD patterns provide evidence for the formation of only a minor amount of crystalline Fe(III) sulfate or hematite directly after the dehydroxylation and dehydration of hydronium jarosite. An *ex situ* XRD study of selected products of the thermal decomposition of hydronium jarosite also failed to positively identify crystalline intermediates [28].

It is possible that any Fe(III) sulfate formed is amorphous. The IES spectra in Fig. 4 clearly show evidence of sulfate bands (1210, 1080 and 1007 cm^{-1}), indicating that the sulfate group has not been changed by thermal treatment at these temperatures. If any hematite is present it is not the major phase, as hematite does not predominate in the XRD patterns until 571 °C. The presence of crystalline $Fe_2O(SO_4)_2$ was not detected. The phases remaining after dehydroxylation and dehydration are most likely an Fe(III) oxy-sulfate compound (stoichiometry unknown) along with a minor amount of hematite. A potential reaction for the decomposition of hydronium jarosite between 300 and 400 °C is given below, along with the empirical formula of the crystalline Fe(III) oxy-sulfate compound:

$$2Fe_3(SO_4)_2(OH)_5 \xrightarrow{300\text{-}400^{\circ}C} 2Fe_3O_{2.5}(SO_4)_2 + 5H_2O$$

Decomposition during the desulfonation stage (500–650 °C) is relatively straightforward in that diffraction peaks for what is presumed to be the Fe(III) oxy-sulfate phase gradually weaken in intensity, while those due to hematite increase in intensity. The major sulfate stretching bands (1210, 1080 and 1007 cm^{-1}) broaden and decrease in intensity until they are no longer detected at 650 °C. It should be noted that librational modes of hydroxyl groups among other modes of vibration also appear in this region and can overlap with the sulfate bands [29]. A band at 1,355 cm^{-1} in the 550 °C spectra, which began as a shoulder in the 350/400 °C spectra becomes more intense. This band is most likely a sulfate band as it is not present in the 700 °C spectra where all sulfate have been decomposed. Thus, the corresponding sulfate group that gives rise to this band at 1,355 cm^{-1} is from a different crystalline phase than the sulfate bands that are observed below 350 °C; most likely what is formed after dehydroxylation and dehydration or an intermediate compound during desulfonation.

The total mass loss due to desulfonation is 30 %, which agrees well with the loss of $2SO_3$ from hydronium jarosite (theoretical mass loss 33 %). Although SO_3 (m/z = 80) is not detected by MS, it

breaks down to SO_2 (m/z = 64) and O_2. Some SO_2 also breaks down to SO (m/z = 48) and O_2. Thus, the decomposition of hydronium jarosite between 500 and 650 °C is represented by the following reaction:

$$2Fe_3O_{2.5}(SO_4)_2 \xrightarrow{500\text{-}650\,^{\circ}C} 3Fe_2O_3 + 4SO_2 + 2O_2$$

This reaction assumes that the material formed after dehydroxylation exists as an oxy-sulfate phase. It should be noted that the hematite bands are located beyond the wavenumber cut-off of the IES employed in this study and are not observed.

Ammoniojarosite thermal decomposition

ICP-OES gave an iron content of 3.01 ± 0.01 in the chemical formula, which is essentially stoichiometric. The N content was determined to be 2.46 % (theoretical 2.92 %). Thus, the amount of NH_4^+ in the chemical formula is 0.88 ± 0.03, with the remainder of the A site assumed to be occupied by hydronium or vacant.

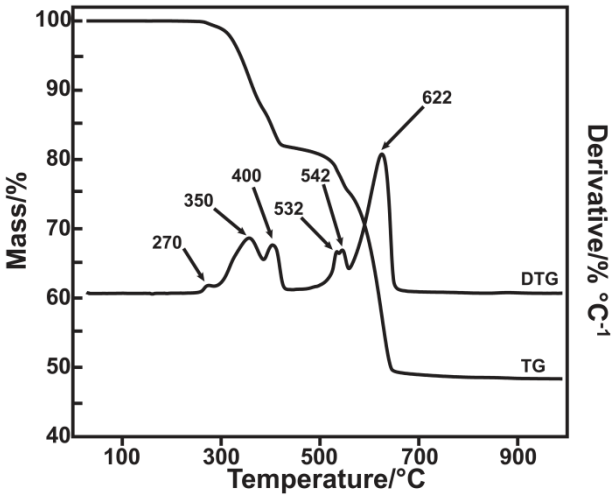

Fig. 5 TG/DTG curves for ammoniojarosite

Thermogravimetric (TG) and differential thermogravimetric (DTG) curves (Fig. 5) indicate that the decomposition of ammoniojarosite occurs in six main steps: 270, 350, 400, 532, 542, and 622 °C. The mass losses are 1, 12, 5, 6 and 27 % (532 and 542 °C combined) respectively. The mass spectra of evolved gases (Fig. 6) shows that the mass loss steps at 350 and 400 °C are due to the simultaneous loss of H_2O (m/z = 18) and NH_3 (m/z = 15). The ion current curve for m/z = 17 originates from both NH_3 and OH^- evolution. The ion current curve m/z = 15 which is due to NH^+ and unique to NH_3, clearly shows that NH_3 is lost simultaneously with H_2O at 350 and 400 °C. Simultaneous evolution of NH_3 and H_2O has been reported for other ammonium-containing minerals such as NH_4^+-vermiculite [30]. Desulfonation occurs at 532, 542 and 622 °C as SO_2, SO, O and S are detected at these temperatures. Full decomposition is completed by 700 °C.

Dehydroxylation, dehydration and deammoniation are completed by about 450 °C. The total mass loss is 51 %.

The temperature maxima of mass loss steps in the dehydration and dehydroxylation region (300–400 °C) for ammoniojarosite are higher than hydronium jarosite by about 20 °C. This could be due to greater proton mobility of hydronium hydrogen atoms compared to ammonium hydrogen atoms. For instance, the hydronium ion has been found to be highly mobile with low activation energy of motion (6.3 kJ mol^{-1}) [31, 32]. Compared to other jarosite minerals, hydronium jarosite is the only end member, which does not show long-range magnetic ordering and is instead, a spin glass [33] which is also related to proton disorder. Given that the pKa of H_3O^+ (0) is much lower than NH_4^+ (9) and both ions surround hydroxyl groups, it is not unreasonable that hydronium jarosite would undergo dehydration and dehydroxylation before ammoniojarosite as the ammonium hydrogen atoms are less mobile and experience less attraction to the surrounding hydroxyl groups.

The small mass loss of 1 % at 270 °C has been assigned to the dehydration of coordinated water, in accordance with the literature [5, 11, 21]. The structure is preserved upon loss of coordinated water, as the diffraction pattern of ammoniojarosite at this temperature shows no evidence for the formation of another phase. While the exact nature of the coordinated water is unknown, the current authors argue that it is related to water or hydronium located at the A site given that there is no signal from *m/z* = 15 at 270 °C. The moles of coordinated water were determined to be 0.26 (~0.25).

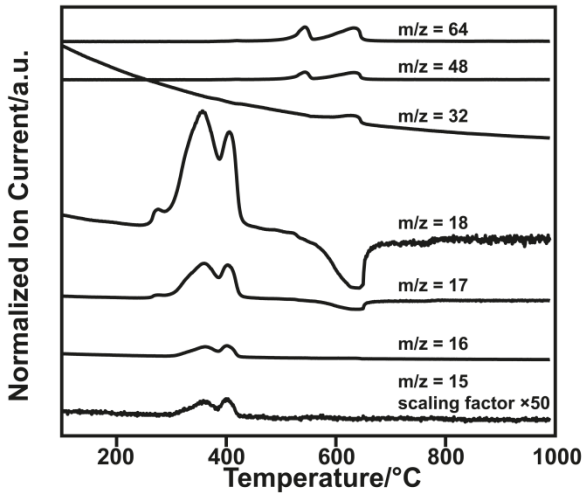

Fig. 6 MS of evolved gases for ammoniojarosite

The TG/DTG curves presented in Fig. 6 are quite different from those reported in another study by Frost et al. [21] for ammoniojarosite. In fact, the TG/DTG curves in the other study are more similar to curves for hydronium jarosite both in this study, and an investigation into hydronium jarosite decomposition also by Frost et al. [17]. The difference in TG/DTG curves could be due to

either ammonium or Fe content. This is because the synthesis employed by Frost et al. [21] used a low concentration of Fe and a high concentration of ammonium ions when compared to the synthesis employed in the current study. Thus, another ammoniojarosite was synthesized using the regime outlined by Frost et al. [21]. The CN analyzer gave a nitrogen content of 0.92 ± 0.04 at the A site (2.69 %); an Fe content of 2.79 ± 0.01 in the chemical formula was found from ICP-OES. Water is known to substitute for Fe^{3+} vacancies in order to maintain charge balance via protonation of OH^- groups [34, 31]. It is proposed that due to extra water being liberated from sites of iron vacancies, the curves reported by Frost et al. [21] appear to be more like hydronium jarosite.

The XRD patterns where there was a change in the diffracting material for ammoniojarosite are shown in Fig. 7. Ammoniojarosite is stable up to 271 °C before a new phase is detected at 321 °C. The pattern at 321 °C also contains some unreacted ammoniojarosite. Like hydronium jarosite, at 720 °C only hematite remains as the pattern is solely due to this phase. The theoretical mass loss with full decomposition of ammoniojarosite to hematite is 50 %, which is in strong agreement with the TG data (a difference of 1 %).

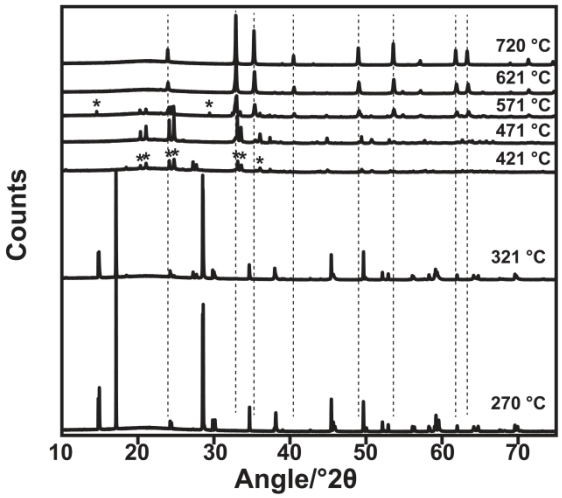

Fig. 7 Significant *in situ* synchrotron XRD patterns of ammoniojarosite (converted to 1.54056 Å) as a function of temperature. Peaks marked with an asterisk at 421 °C are from $FeSO_4$ and those at 571 °C are from $Fe_2(SO_4)_3$. Most intense hematite peaks are marked with a dashed line

IES spectra of ammoniojarosite at various temperatures are shown in Fig. 8. The band at 1,420 cm^{-1} is assigned to an NH_4^+ deformation vibration in agreement with other spectroscopic studies of ammoniojarosite [35, 36]. This band persists until 350 °C but completely disappears by 400 °C. A band at 1,640 cm^{-1} is most likely due to an O–H bending vibration [27, 29, 37, 38] as this band is also in the hydronium jarosite spectra. The O–H and N–H stretching vibrations are gone by 500 °C. The IES spectra of O–H and N–H bending modes are in agreement with the simultaneous loss of NH_3 and H_2O as argued from the MS analysis of evolved gases, and also the IES spectra of Frost et al. [21].

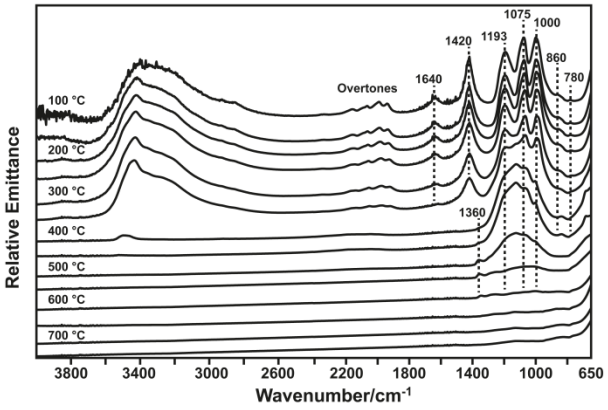

Fig. 8 IES spectra of ammoniojarosite (4,000 – 650 cm^{-1})

If ammoniojarosite decomposes to release $3.5H_2O$ and $1NH_3$ [7] by 400 °C, then the theoretical mass loss is 16.9 % which is in close agreement with the observed mass loss of 17 %. Thus, dehydroxylation and dehydration are completed before desulfonation as all hydrogen atoms have been lost from the structure. The exact mechanism by which this occurs is unclear from synchrotron XRD as the phases formed were not positively identified. It is argued that the evolution of NH_3 would happen similar to the first mass loss step of hydronium jarosite: NH_4^+ protonates a surrounding hydroxyl group to form NH_3 and H_2O which are then liberated. An overall equation for the dehydroxylation, dehydration and deammoniation of ammoniojarosite is given by:

$$2NH_4Fe_3(SO_4)_2(OH)_6 \xrightarrow{300\text{-}400^{\circ}C} 7H_2O + 2NH_3 + 2Fe_3O_{2.5}(SO_4)_2$$

The 532 and 542 °C steps in desulfonation (Fig. 5) correspond to a two step degradation of the oxy-sulfate phase/s remaining after dehydration, dehydroxylation, and deammoniation. Similar to hydronium jarosite, crystalline Fe(III) sulfate is not detected directly after deammoniation and dehydroxylation. A sulfate band due to different crystalline phases is also seen at 1,360 cm^{-1}. At 421 °C iron (II) sulfate ($FeSO_4$) was identified. It is also present until 521 °C before Fe(III) sulfate [$Fe_2(SO_4)_3$] is detected at 571 °C. Hematite predominates at 621 °C, but unlike hydronium jarosite where the most intense hematite peaks are only just resolved above background, in ammoniojarosite they are clearly present at 521 °C. The detection of $FeSO_4$ is unexpected as well as the subsequent transformation to $Fe_2(SO_4)_3$. However, as the atmosphere in the capillary was not controlled; it is conceivable that any oxygen (O_2) previously present would result in the oxidation of $FeSO_4$ to $Fe_2(SO_4)_3$ and Fe_2O_3. This explains the earlier detection of hematite when compared to hydronium jarosite.

It is often assumed that $Fe(OH)SO_4$ and $Fe_2O(SO_4)_2$ are formed during the thermal decomposition of ammoniojarosite [4, 11]. Ristić et al. [4] found evidence of the formation of these two iron

compounds at 400 °C using Mössbauer spectroscopy. These two compounds were unable to be positively identified from synchrotron XRD due to the lack of reference patterns. Alternatively, it is possible that the $FeSO_4$ formed in the current study is due to the dehydroxylation of intermediate amorphous $Fe(OH)SO_4$ and $Fe_2O(SO_4)_2$ phases.

Fe(II) sulfate is rarely proposed as an intermediate in jarosite mineral decomposition as the Fe(III) in jarosite must be reduced and then oxidized again to form hematite. However, Fe(III) reduction to Fe(II) during thermal decomposition has been reported for ammonium fluoroferrates [39], various Fe(III) oxalates [40] and during Fe^{3+} exchange for NH_4^+ in Na^+-Fe^{3+} ZSM-5 zeolites [41]. The reduction of Fe(III) to Fe(II) for Fe(III) oxalates was also accompanied by the subsequent oxidation of Fe(II) to Fe(III) via formation of Fe(III) oxide as the temperature increased [40]. In the present study, the reduction of Fe(III) is most likely due to a redox reaction involving Fe(III) and the liberated NH_3 to form Fe(II) and N_2. The reduction could be initiated by NH_3 itself, or the result of a catalytic decomposition of NH_3 by Fe [41].

This redox reaction happens in a closed environment, for example a capillary, because the liberated NH_3 does not easily diffuse away from the sample and is available to react. It is the opinion of the current authors that an *in situ* XRD experiment performed under both air and an inert atmosphere such as Ar or N_2 where any liberated gases are carried away from the sample surface may help to resolve these issues. Following the formation of $Fe_2(SO_4)_3$, the decomposition is straightforward and proceeds by the evolution of SO_3 ($SO_2 + O_2$) to form hematite.

In order to determine whether Fe(II) could be detected outside of the synchrotron experiment, a sample of ammoniojarosite was heated in a tubular furnace under a slight positive pressure of Ar at 500 °C for 1 h. An additional sample of ammoniojarosite was heated in a capillary sealed with Blu-Tack at one end with heating (500 °C for 5 min) provided by a hot air gun, in order to recreate the conditions of the synchrotron experiment. The resultant solids from both heating regimes were digested in sulfuric acid, adjusted to pH 4 with ammonium acetate/acetic acid buffer, followed by addition to a 3 g L^{-1} 1,10-phenanthroline solution. This test is well known to be an indicator for the presence of Fe(II), with a positive result being a color change of the solution to orange [42].

The sample of ammoniojarosite heated under Ar in the tube furnace tested negative for Fe(II), whilst the sample heated with the hot air gun gave a positive test. Thus, there is evidence for the presence of Fe(II) ions in the form of Fe(II) sulfate. This experiment suggests that the Fe(II) ions are formed due to a redox reaction between iron and the liberated NH_3. No such reaction occurs in the tube furnace, TG or IES as the liberated NH_3 is free to diffuse away from the sample and into the carrier gas. In a well-packed capillary however, the NH_3 is available to interact with the sample and promote the reduction of Fe(III) to Fe(II).

Conclusions

The thermal decomposition of hydronium jarosite and ammoniojarosite has been investigated using TG/MS, in situ synchrotron XRD and IES. The crystalline intermediate compounds formed during decomposition, were in general, not positively identified. Other previously reported intermediates for ammoniojarosite and hydronium jarosite decompositions most likely exist as amorphous phases or alternate phases to what is contained in powder diffraction databases. IES data with support from TG/MS show that the hydronium ion does not persist in the crystal structure past 400-450 °C and that no water is evolved during the desulfonation stage. The evolution of ammonia and water are simultaneous in ammoniojarosite. Both Fe(II) sulfate and Fe(III) sulfate were detected in the synchrotron XRD patterns of ammoniojarosite at 421 °C and 571 °C respectively. The initial presence of Fe(II) sulfate is most likely due to a redox reaction involving Fe(III) and the liberated NH_3. The subsequent formation of Fe(III) sulfate can be explained by the reaction of Fe(II) sulfate with O_2 to also form hematite. The presence of Fe(II) ions were confirmed by the 1,10-phenanthroline test for ammoniojarosite that was heated in a similar fashion at the synchrotron, as the liberated NH_3 cannot diffuse away from the sample. It was also suggested that low Fe occupancy may change the appearance of TG/DTG curves to be more like hydronium jarosite. The utility of *in situ* X-ray diffraction for determining decomposition products is clearly demonstrated by the detection, or lack thereof, of crystalline phases that were at odds with those previously proposed. However, the positive identification of crystalline intermediates, especially of intermediate products, is more challenging.

Acknowledgements

Part of this research was undertaken on the Powder Diffraction beam line at the Australian Synchrotron, Victoria, Australia. The authors acknowledge travel funding provided by the International Synchrotron Access Program (ISAP) which is managed by the Australian Synchrotron and funded by the Australian Government. The financial and infrastructure support from the Queensland University of Technology is gratefully acknowledged. The Australian Institute of Nuclear Science and Engineering (AINSE) and the Australian government are also acknowledged for financial support.

References

1. Dutrizac JE. Factors affecting the precipitation of potassium jarosite in sulfate and chloride media. Metall Mater Trans B. 2008;39(6):771-83.
2. Hochella Jr MF, Moore JN, Putnis CV, Putnis A, Kasama T, Eberl DD. Direct observation of heavy metal-mineral association from the Clark Fork River Superfund Complex: implications for metal transport and bioavailability. Geochim Cosmochim Acta. 2005;69(7):1651-63.

3. Kubisz J. Studies on synthetic alkali-hydronium jarosites II: thermal investigations. Mineral Pol. 1971;2:51-9.
4. Ristić M, Musić S, Orehovec Z. Thermal decomposition of synthetic ammonium jarosite. J Mol Struct. 2005;744-747:295-300.
5. Alonso M, López-Delgado A, López FA. A kinetic study of the thermal decomposition of ammoniojarosite. J Mater Sci. 1998;33:5821-5.
6. Swamy MSR, Prasad TP, Sant BR. Thermal analysis of ferrous sulphate heptahydrate in air. Part I: some general remarks and methods. J Therm Anal. 1979;15:307-14.
7. Kunda W, Veltman H. Decomposition of jarosite. Metall Trans B. 1979;10B:439-46.
8. May A, Sjoberg JJ, Baglin EG. Synthetic argentojarosite: physical properties and thermal behaviour. Am Miner. 1973;58:936-41.
9. Kotler JM, Hinman NW, Richardson CD, Scott JR. Thermal decomposition behavior of potassium and sodium jarosite synthesized in the presence of methylamine and alanine. J Therm Anal Calorim. 2010;102:23-9.
10. López-Delgado A, López FA. Thermal decomposition of ferric and ammonium sulphates obtained by bio-oxidation of water pickling liquors with *Thiobacillus ferroxidans*. J Mater Sci. 1995;30:5130-8.
11. López-Delgado A, Alguacil FJ, López FA. Recovery of iron from bio-oxidized sulphuric pickling waste water by precipitation as basic sulphates. Hydrometallurgy. 1997;45:97-112.
12. Chio CH, Sharma SK, Ming L-C, Muenow DW. Raman spectroscopic investigation on jarosite-yavapaiite stability. Spectrochim Acta A. 2010;75:162-71.
13. Drouet C, Navrotsky A. Synthesis, characterization, and thermochemistry of K-Na-H_3O jarosites. Geochim Cosmochim Acta. 2003;67(11):2063-76.
14. Xu H, Zhao Y, Vogel SC, Hickmott DD, Daemen LL, Hartl MA. Thermal expansion and decomposition of jarosite: a high-temperature neutron diffraction study Phys Chem Miner. 2010;37:73-82.
15. Vassallo AM, Finnie KS. Infrared emission spectroscopy of some sulfate minerals. Appl Spectrosc. 1992;46:1477-82.
16. Drouet C, Pass KL, Baron D, Draucker S, Navrotsky A. Thermochemistry of jarosite-alunite and natrojarosite-natroalunite solid solutions. Geochim Cosmochim Acta. 2004;68(10):2197-205.
17. Frost RL, Wills R-A, Kloprogge JT, Martens WN. Thermal decomposition of hydronium jarosite $(H_3O)Fe_3(SO_4)_2(OH)_6$. J Therm Anal Calorim. 2006;83:213-8.
18. Hartman M, Veselý V, Jakubec K. Thermal decomposition and chemism of hydronium jarosite. Collect Czech Chem Commun. 1987;52:939-48.
19. Šolc Z, Trojan M, Brandová D, Kuchler M. A study of hydrothermal preparation of iron(III) pigments by means of thermal analysis methods. J Therm Anal. 1988;33(463-469).
20. Das GK, Anand S, Acharya S, Das RP. Preparation and decomposition of ammoniojarosite at elevated temperatures in H_2O-$(NH_4)_2$-SO_4-H_2SO_4 media. Hydrometallurgy. 1995;38:263-76.
21. Frost RL, Wills R-A, Kloprogge JT, Martens W. Thermal decomposition of ammonium jarosite $NH_4Fe_3(SO_4)_2(OH)_6$. J Therm Anal Calorim. 2006;84:489-96.

22. Basciano LC, Peterson RC. Jarosite-hydronium jarosite solid-solution series with full iron site occupancy: mineralogy and crystal chemistry. Am Mineral. 2007;92:1464-73.
23. Stoffregen RE, Alpers CN, Jambor JL. Alunite-jarosite crystallography, thermodynamics, and geochronology. Rev Mineral Geochem. 2000;40:453-79.
24. Frost RL, Vassallo AM. The dehydroxylation of the kaolinite clay minerals using infrared emission spectroscopy. Clay Clay Miner. 1996;44(5):635-51.
25. Kubisz J. Studies on synthetic alkali-hydronium jarosites III: infrared absorption study. Mineral Pol. 1972;3:23-37.
26. Grohol D, Nocera DG. Magnetic disorder in the frustrated antiferromagnet jarosite arising from the H_3O^+•••OH^- interaction. Chem Mater. 2007;19(12):3061-6.
27. Wilkins RWT, Mateen A. The spectroscopic study of oxonium ions in minerals. Am Mineral. 1974;59:811-9.
28. Majzlan J, Stevens R, Boerio-Goates J, Woodfield BF, Navrotsky A, Burns PC et al. Thermodynamic properties, low-temperature heat-capacity anomalies, and single-crystal X-ray refinement of hydronium jarosite, $(H_3O)Fe_3(SO_4)_2(OH)_6$. Phys Chem Miner. 2004;31(8):518-31.
29. Powers DA, Rossman GR, Schugar HJ, Gray HB. Magnetic behavior and infrared spectra of jarosite, basic iron sulfate, and their chromate analogs J Solid State Chem. 1975;13:1-13.
30. Pérez-Rodríguez JL, Poyato J, Jiménez de Haro MC, Pérez-Maqueda LA, Lerf A. Thermal decomposition of NH_4^+-vermiculite from Santa Olalla (Huelva, Spain) and its relation to the metal ion distribution in the octahedral sheet. Phys Chem Miner. 2004;31:415-20.
31. Nielsen UG, Heinmaa I, Samoson A, Majzlan J, Grey CP. Insight into the local magnetic environments and deuteron mobility in jarosite $(AFe_2(SO_4)_2(OD,OD_2)_6$, A = K, Na, $D_3O)$ and hydronium alunite $((D_3O)Al_3(SO_4)_2(OD)_6)$, from variable-temperature ^2H MAS NMR spectroscopy. Chem Mater. 2011;23:3176-87.
32. Nielsen UG, Majzlan J, Grey CP. Determination and quantification of the local environments in stoichiometric and defect jarosite by solid-state 2H NMR spectroscopy. Chem Mater. 2008;20(6):2234-41.
33. Wills AS, Harrison A. Structure and magnetism of hydronium jarosite, a model Kagomé antiferromagnet. J Chem Soc Faraday Trans. 1996;92:2161-6.
34. Frunzke J, Hansen T, Harrison A, Lord JS, Oakley GS, Visser D et al. Magnetic ordering in dilute kagome antiferromagnets. J Mater Chem. 2001;11:179-85.
35. Sasaki K, Tanaike O, Konno H. Distinction of jarosite-group compounds by Raman spectroscopy. Can Mineral. 1998;36:1225-35.
36. Serna CJ, Cortina CP, Garcia Ramos JV. Infrared and Raman study of alunite-jarosite compounds. Spectrochim Acta A. 1986;42A:729-34.
37. Bishop JL, Murad E. The visible and infrared spectral properties of jarosite and alunite. Am Mineral. 2005;90:1100-7.
38. Makreski P, Jovanoski G, Dimitrovska S. Minerals from Macedonia XIV. Identification of some sulfate minerals by vibrational (infrared and Raman) spectroscopy. Vib Spec. 2005;39:229-39.

39. Laptash NM, Polyshchuk SA. Thermal decomposition of ammonium fluoroferrates $(NH_4)_xFeF_{2x}$ $(2 \leq x \leq 3)$. J Therm Anal. 1995;44:877-83.
40. Gallagher PK, Kurkjian CR. A study of the thermal decomposition of some complex oxalates of iron(III) using the Mössbauer effect. Inorg Chem. 1966;5:214-9.
41. Kaliaguine S, Lemay G, Adnot A, Burelle S, Audet R, Jean G et al. Ion exchange of Fe^{3+} in ZSM-5. Zeolites. 1990;10:559-64.
42. ASTM Standard E394. Standard test method for iron in trace quantities using the 1,10-phenanthroline method. West Conshohocken, PA: ASTM International; 2009.